

A traction force approach for fatigue assessment of complex welded structures

Matti Rautiainen^{1,2}  | Heikki Remes¹ | Ari Niemelä²

¹Department of Mechanical Engineering,
 Aalto University School of Engineering,
 Espoo, Finland

²Structural Design, Meyer Turku Oy,
 Turku, Finland

Correspondence

Matti Rautiainen, Department of
 Mechanical Engineering, Aalto University
 School of Engineering, P.O. Box 15300,
 Espoo 02150, Finland.
 Email: matti.rautiainen@aalto.fi

Funding information

Meyer Turku Oy

Abstract

A new traction force approach (TFA) for weld root fatigue analysis of complex cruciform connections is introduced. The approach defines the local nominal weld stress by using a solid element model and connecting the welded parts only from the toe and root lines. This enables the peak weld forces to be distinctly defined. The TFA approach was validated with a fully connected solid element model. As a comparison, the same analyses were performed for a shell element model. The study shows that the approach that is introduced here gives a good estimate for the local weld force with a maximum error of 10% while the commonly used shell element model greatly overestimates the peak weld force, particularly for complex connections. The analysis of fatigue-tested connections showed that by using TFA, instead of an approach based on overall nominal weld stress, the scatter range index is reduced from 3.71 to 1.98. The TFA approach is much more efficient compared to conventional approaches because of the low pre- and post-processing effort.

KEY WORDS

fatigue life prediction, fatigue of welds, finite element analysis, welded structures

1 | INTRODUCTION

In welded structures, where scantlings are defined on the basis of stability or stiffness criteria, e.g., buckling, welded connections do not necessarily require matching strength with the connected member. If a high number of such joints exists, considerable production savings can be achieved by reducing the number of welded stiffeners and by using single bead fillet welds instead of, e.g., full penetration welds. This often means that the joint becomes unsymmetrical and the fatigue strength of the connection is seriously affected as the fatigue initiation site changes from the weld toe to the weld root. As a consequence, fatigue analysis becomes more challenging,

especially in large structures such as a ship hull or a steel bridge, where the connection between the structural members is complex. Complex connections have a lack of symmetry planes, eccentricity of welds, thin intermediate plates, and stress concentrations as a result of the intersecting welds. One example of such a connection can be found in cruise ships, where a rectangular pillar is welded to the deck and sides of the RHS profile are aligned with an underlying web, girder, and flat bar; see Figure 1. With such a light structural arrangement, sufficient strength can be achieved since the pillar loading is not significant. However, at present, the time-efficient fatigue design methods needed for the structural optimization and for the approval process with classification

This is an open access article under the terms of the Creative Commons Attribution License, which permits use, distribution and reproduction in any medium, provided the original work is properly cited.

© 2021 The Authors. *Fatigue & Fracture of Engineering Materials & Structures* published by John Wiley & Sons Ltd.

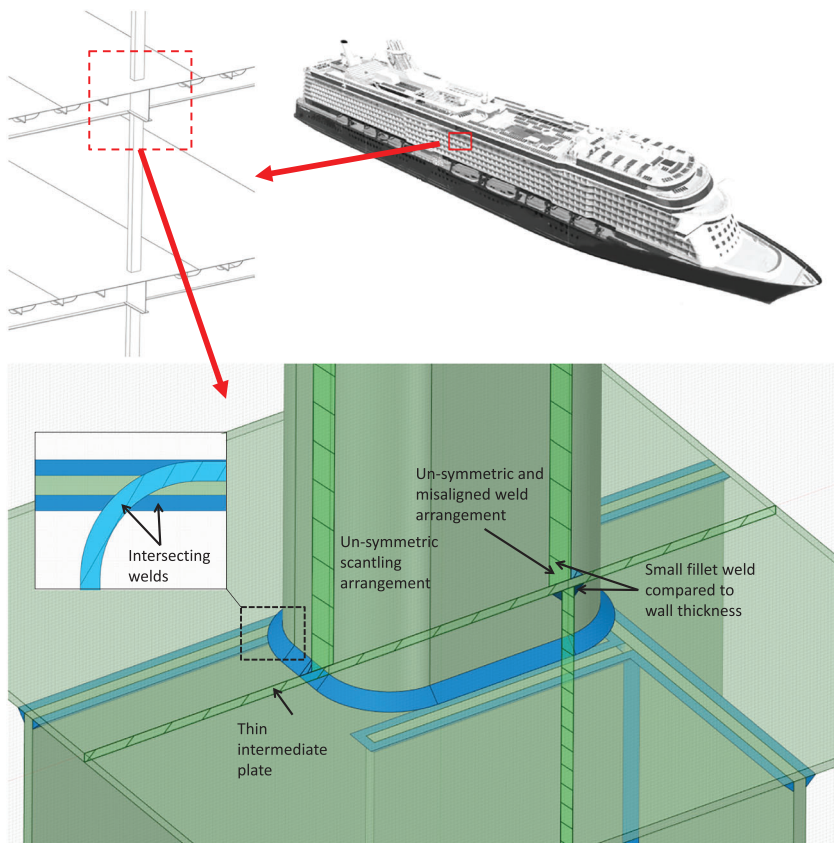


FIGURE 1 An example of complex fillet welded joints, where weld root fatigue is the dominant failure mode [Colour figure can be viewed at wileyonlinelibrary.com]

societies do not exist for such complex connections. Considering that structural analysis is carried out using the finite element (FE) method, an efficient design method should be insensitive to element type, size, and shape. Additionally, the post-processing of the results should be simple and straightforward in order to make the method suitable for structural optimization.

According to present fatigue design standards and recommendations, the nominal weld stress approach is the most commonly adapted approach for the fatigue analysis of a weld root.^{1–4} The nominal weld stress is defined as the averaged stress at the weld

$$\sigma_w = \frac{F}{\Sigma(a_w l)}, \quad (1)$$

where F is the total transmitted force, a_w the throat thickness, and l the total weld length l . In fillet welds around loaded attachment ends, the effective area and force should be used.⁵ For more complex filled welded joints, the definition of the nominal weld stress is a challenge, and thus, the use of local approaches such as effective notch stress (ENS) or structural weld stress is recommended.^{3,4}

The most common local approach is ENS. In ENS, a welded joint is modeled with solid or 2D elements,

including the weld geometry with a 1-mm radius at the weld toe and root. Since a very small element size, i.e., a quarter of the radius for higher order elements, is required, this approach is very time-consuming for complex structures. Furthermore, it is observed that ENS is sensitive to the element mesh and the applied sub-modeling technique in the case of 3D structures.^{6,7} To avoid the modeling of the weld radius, the peak stress method⁸ can be used. It uses solid FE models to calculate the notch stress intensity factor at the weld root or toe, and thus, the weld root can be modeled with a zero radius, making the geometry modeling straightforward. In the peak stress method, the element size can vary from 0.4 to 2 mm. The disadvantage is that the method is sensitive to the selected element type and FE software. Fatigue assessment of a weld root can also be performed using the strain energy density (SED) approach.^{9,10} It derives from the theory that the high cycle fatigue of steels is driven by the critical value of the averaged strain energy density at the control volume around the notch tip. When applying SED to the FE method, the control volume, with a radius of, e.g., 0.28 mm, is meshed with a fine or coarse mesh. As in the peak stress approach, SED uses a zero radius to model the notch tip, making the geometry modeling straightforward. However, in large and complex structures, challenge is that the required

element size can be very small compared to overall dimensions of the structure. As a large structure such as shown in Figure 1 cannot be modeled with so small element size, it is challenging to control the element size to be changed from micrometer scale to millimeter or centimeter scale. To achieve a smooth transition between these element sizes, the number of elements can increase beyond what is reasonable to be analyzed. This issue concerns also all crack initiation and propagation approaches.^{11,12}

Using a structural weld stress approach, the element size requirement can be relaxed. In a structural weld stress approach, the stress is calculated at the weld root by considering both the weld membrane stress and the linearly distributed bending stress. For defining the structural weld stress using FE modeling, different approaches have been presented. Sorensen et al.¹³ used the linear extrapolation of the principal stress at the fillet weld throat section to capture the bending effect, while Fricke¹⁴ suggests that the weld leg section perpendicular to the load should be used to calculate the weld root structural stress as the fatigue crack path is closer to that. To avoid a stress singularity problem at the sharp weld notch, the traction structural stress approach, based on nodal forces, is also introduced.¹⁵ Although all these structural weld stress approaches are highly appreciated, they are still challenging in terms of the post-processing of the nodal forces to define the stress at the weld leg section. In complex geometries using automatic FE meshing, nodes are often positioned inconsistently along the weld surface, making automated post-processing difficult. Furthermore, the critical position, i.e., the place where there is the maximum stress, is impossible to predict before FE analysis. Therefore, there is a need for local nominal or structural stress approaches that can efficiently analyze all the fillet welded joints in complex structures.

In this paper, a new approach is introduced for calculating the local nominal weld stress of complex load-carrying cruciform connections. The modeling technique uses nodal traction forces. Differently from the existing methods, fillet welds are connected only from their root and toe borderlines. As a result, the weld forces are easily captured, and the local nominal stress at the welded joint is defined with minor post-processing work. In this work, the traction force approach (TFA) is applied for various filled weld configurations. The approach is shown to be accurate and independent of element size, making it suitable for automated FE modeling and optimizing structural arrangement in welded connections.

This paper has the following structure and content. First, the method which TFA is based on is introduced in Section 2. Section 3 explains the complex connections selected for validation. The TFA approach is validated

with a fully connected solid element model and compared to the shell modeling approach. The results, e.g., the accuracy of the TFA, is shown in Section 4. This section also includes a comparison in terms of fatigue test data. Sections 5 and 6 include the discussion and conclusions.

2 | TRACTION FORCE APPROACH

2.1 | Modeling principle

The purpose of the TFA approach is to solve the force components (i.e., normal and shear forces) acting locally on a weld in a way that is easy to apply in FE modeling. These force components are used for calculating the nominal weld stress for the local nominal weld stress fatigue approach.

In a general case, a fillet welded connection is loaded by external forces and bending moments as shown in Figure 2A. Considering the weld leg section, the external loading is transmitted from one structural member to another by the normal force N_z , longitudinal shear force Q_x , transverse shear force Q_y , and bending moment M_x . The normal force N_z and bending moment M_x induce nonlinear normal stress distribution in the weld leg section. The shear stress τ_{xy} is induced by the longitudinal shear force Q_x and the shear stress τ_{yz} by the transverse shear force Q_y . The stress state is shown schematically in Figure 2B. In general, a welded connection can also be loaded by the longitudinal normal force. However, since this loading component is not transmitted from one structural member to another by a weld, it is not considered here.

In order to get distinct weld force readings, a pointwise (or linewise in 3D) connection is needed between the weld and the connected plate. Also, to solve the correct transmission of the force from the welds on one side of an intermediate plate to another, the bending stiffness of the welds needs to be included in the connection. This is also required to solve the correct force distribution along the weld length in complex welded joints.

The principle in TFA is to model the contact of the weld leg section with two pivot points, i.e., the root and toe point. As a result, the pivot points will have three force components acting on them, i.e., the normal forces $N_{z,t}$ and $N_{z,r}$, the shear forces $Q_{y,t}$ and $Q_{y,r}$, and the shear forces $Q_{x,t}$ and $Q_{x,r}$ (see Figure 2C). TFA is used for finding the normal force N_z , the shear forces Q_x and Q_y , and the bending moment M_x .

$$N_z = N_{z,t} + N_{z,r}, \quad (2)$$

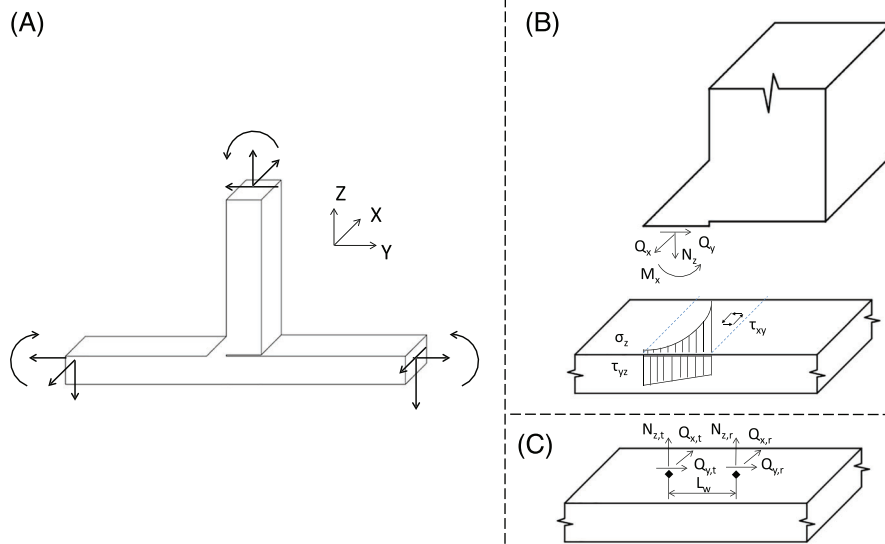


FIGURE 2 General loading of welded connection (A) and stress state at weld leg section (B). Force components for TFA (c) [Colour figure can be viewed at wileyonlinelibrary.com]

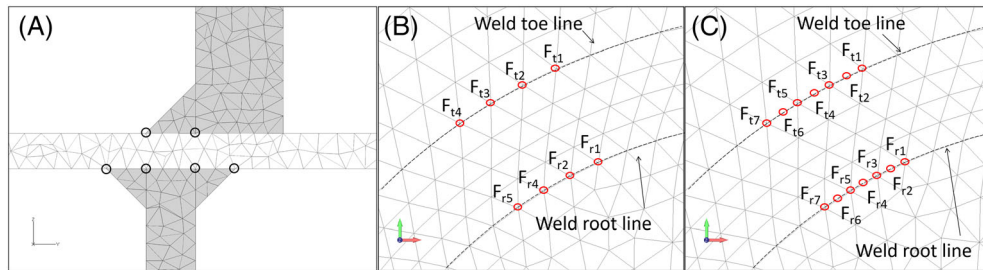


FIGURE 3 Connected nodes in TFA (A) and corresponding nodal forces with linear elements (B) and parabolic elements (C) [Colour figure can be viewed at wileyonlinelibrary.com]

$$Q_x = Q_{x,t} + Q_{x,r}, \quad (3)$$

$$Q_y = Q_{y,t} + Q_{y,r}, \quad (4)$$

$$M_x = 0.5L_w(N_{z,t} - N_{z,r}). \quad (5)$$

2.2 | FE implementation

Applying TFA to FE modeling is explained here. In a structural design process, a 3D geometry model of the structure is typically created, making the implementation of TFA particularly simple. The geometry model should include the weld geometry, and it should be modeled with solid elements in order to model correctly the force transmission in complex welded connections. Therefore, 3D geometry is not modified into a mid-surface model as in shell modeling. Since hexahedron meshing is challenging for complex welded connections, in TFA, the connection is modeled with tetrahedron elements. Before automated mesh generation is used, the node specification (number or spacing) is only added to the borderlines of the weld toe and root. In the model, the abutting parts

will have a continuous mesh with the fillet welds, as highlighted in gray in Figure 3A. The abutting structure is then connected to the intermediate plate by merging the nodes at the toe and root borderlines. To prepare the geometry model for meshing, the surfaces of the intermediate plate and weld leg section need to have imprinted lines at the weld toe and root. This can be done by utilizing the geometry of the abutting structure. In order to correctly sum up the nodal forces at the root and toe lines, as per Equations 2–4, an equal number of nodes needs to be set on these lines. The element size is selected to be such as to maintain good element quality in automated mesh generation. The following bullet points give guidelines for FE modeling with the traction force approach.

- Obtain a 3D model of the structure, including weld geometries.
- Set a continuous mesh for the abutting structural member and the weld.
- Utilizing the geometry model of the abutting structure, imprint weld root and toe lines on the intermediate plate and weld leg surface.
- Set a constant element size over the connection region.

- If needed, adjust the mesh so that an equal number of elements is created along the root and toe line.
- After meshing, utilizing the imprinted line geometries, merge the nodes along the weld root and toe lines.

In the post-processing phase, the forces and moment as per Equations 2–5 are calculated element-wise along the weld length, using nodal forces F_i (Figure 3B,C), the distances D_i between nodes and the weld leg length L_w . Considering here only the normal force (Equation 2) and bending moment (Equation 5), the element-wise solution for 3D-structures is the line traction force f_l and line bending moment m_l shown in Table 1. The line traction force is calculated by dividing the combined elemental force at weld toe and root line by the average element length at weld toe and root line. For linear elements, the elemental force is the average of element corner node forces (e.g., F_{r2} and F_{r3} for weld root line). With parabolic elements, the mid-node force is added. From the line traction force, elemental nominal weld stress σ_w is calculated according to the definition of IIW.⁴ For the line bending moment m_l , bending moment calculated from elemental weld toe and root forces is divided by the average element length at weld toe and root line. All equations, f_l , m_l , and σ_w , are presented for both linear and parabolic elements in Table 1.

3 | VALIDATION OF THE TRACTION FORCE APPROACH

3.1 | Selected welded connections

The proposed TFA approach is validated with the nine complex load-carrying welded connections reported in Table 2. The selected connections are arranged in order of increasing complexity. The first three cases are symmetrical connections, for which fatigue tests are available from the previous investigation.^{14,16} Cases 4 to 9 are more complex unsymmetrical connections with a more pronounced 3D effect. As shown in Figure 1, such a connection can be found on cruise ships, where a rectangular pillar is welded to the deck, aligning the sides of the RHS profile with an underlying web, girder, and flat bar. It is

possible to put such a complex structure with a thin intermediate plate into practice when the pillar load is not significant. Moreover, cases 7 and 9 represent situations where the pillar is positioned eccentrically because of manufacturing tolerances. A graphic representation of these connections can be seen in Figure 4, while detailed test specimen dimensions for cases 1–3 can be found from the original papers. The material of all the case connections is steel with a Young's modulus $E = 210$ GPa and Poisson's ratio $\nu = 0.3$. A more thorough description of the connections is given below.

In case 1, RHS-120x80x6 profiles are welded onto a 15-mm intermediate plate using fillet welds with a mean throat thickness of 4.7 mm, as shown in Figure 4A.¹⁴ The connection is loaded with an X-axis three-point bending load. In such a connection, only a slight weld force concentration is induced to the corners of the RHS profile, making the structural analysis with beam theory possible with reasonable accuracy. In cases 2 and 3, the level of complexity is increased as they have welds intersecting at a 90° angle, creating a severe weld force concentration at the intersection point. In case 2, the axial load is applied on 6-mm-thick plates welded onto a 6-mm-thick intermediate plate and a 10-mm-thick cover plate (Figure 4B).¹⁴ The loaded plates are positioned at a 90° angle. The failed fillet welds between the cover plate and intermediate plate have a mean throat thickness of 4.3 mm. In case 3, a Ø76.1 × 2.9 tube is welded between HEA200 profiles, which are cut in half (Figure 4C).¹⁶ An axial load is applied to the side surfaces of the HEA web plate as the force is transmitted to the HEA profile through the friction force. A weld stress concentration is created at the point where the tube weld intersects with the web of the HEA profile. The weld profile is a partial penetration weld reinforced with a fillet weld with a total mean throat thickness of 6.0 mm and a weld leg length of 8.2 mm. Case 3 has a more severe stress concentration than case 2 because of the longer weld length.

In addition to symmetrical fatigue-tested connections (cases 1 to 3), the proposed TFA is validated with six unsymmetrical and more complex connections. Cases 4 to 9 have an RHS-150 × 100 × 12.5 profile welded to an intermediate plate supported by an unsymmetrical 7-mm-thick plate structure. The edges of the intermediate plate and the

TABLE 1 Equations for line traction force f_l , line bending moment m_l and nominal weld stress σ_w

Linear elements	Parabolic elements
$f_{li,i+1} = \frac{F_r + F_{ri+1} + F_u + F_{ui+1}}{D_{ri,i+1} + D_{ui,i+1}}$	$f_{li,i+2} = \frac{F_r + 2F_{ri+1} + F_{ri+2} + F_u + 2F_{ui+1} + F_{ui+2}}{D_{ri,i+2} + D_{ui,i+2}}$
$m_{li,i+1} = \frac{L_w(F_r + F_{ri+1} - F_u - F_{ui+1})}{D_{ri,i+1} + D_{ui,i+1}}$	$m_{li,i+2} = \frac{L_w(F_r + 2F_{ri+1} + F_{ri+2} - F_u - 2F_{ui+1} - F_{ui+2})}{D_{ri,i+2} + D_{ui,i+2}}$
$\sigma_{wi,i+1} = \frac{f_{li,i+1} * 1mm}{a_w}$	$\sigma_{wi,i+2} = \frac{f_{li,i+2} * 1mm}{a_w}$

TABLE 2 Case connections for validation

Case	Profile	Supporting structure	IP thickness [mm]	Profile weld	Supporting structure weld	Number of symmetry planes in connection	Loading type	Profile positioned symmetrically with supporting structure
1	RHS-120x80x6	RHS-120x80x6	15	Variet SSFW	Variet SSFW	2	4kN load, 3-point bending	YES
2	Plate-80x80x6	Plate-80x80x6	6 and 10	Variet DFW	Variet DFW	2	1kN axial load	YES
3	CHS-76.1x2.6	HEA200 web plate, $t = 6.5$ mm	10	Variet SSPP+FW	-	1	2kN axial load NO, 1.95 mm offset	
4	RHS-150x100x12.5	Plate intersection, $t = 7$ mm	10	a5 SSFW	a4 DFW	0	1kNm bending moment	YES
5	RHS-150x100x12.5	Plate intersection, $t = 7$ mm	5	a5 SSFW	a4 DFW	0	1kNm bending moment	YES
6	RHS-150x100x12.5	Plate intersection, $t = 7$ mm	10	a5 SSFW	a4 DFW	0	1kN axial load	YES
7	RHS-150x100x12.5	Plate intersection, $t = 7$ mm	10	a5 SSFW	a4 DFW	0	1kN axial load	NO, 7 mm offset
8	RHS-150x100x12.5	Plate intersection, $t = 7$ mm	5	a5 SSFW	a4 DFW	0	1kN axial load	YES
9	RHS-150x100x12.5	Plate intersection, $t = 7$ mm	5	a5 SSFW	a4 DFW	0	1kN axial load	NO, 7 mm offset

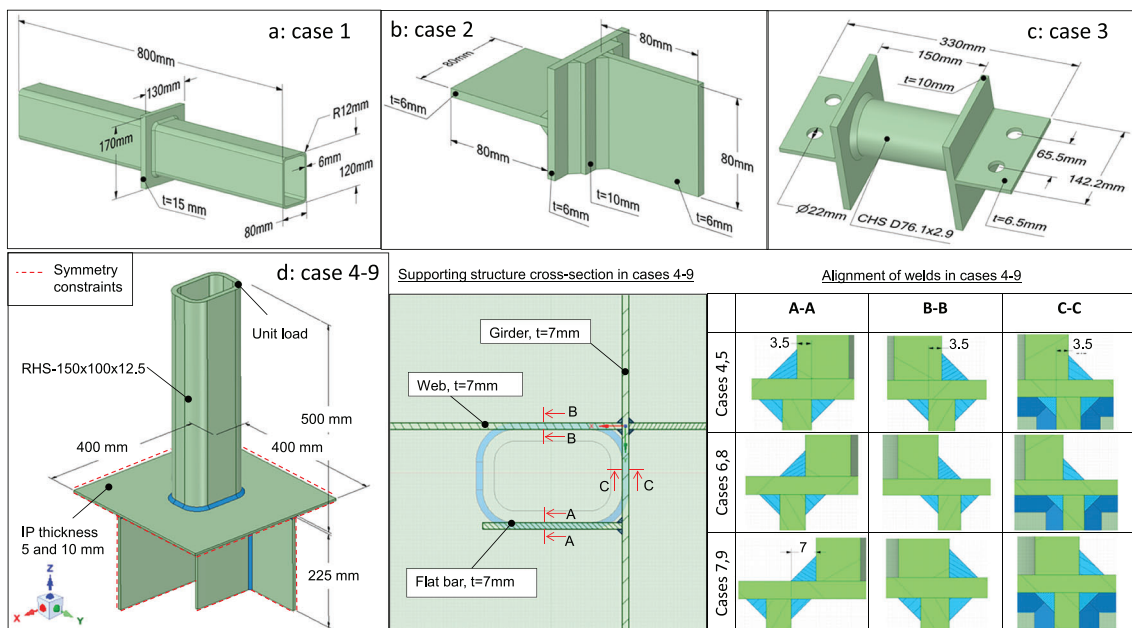


FIGURE 4 Geometry of case connections 1 to 9 [Colour figure can be viewed at wileyonlinelibrary.com]

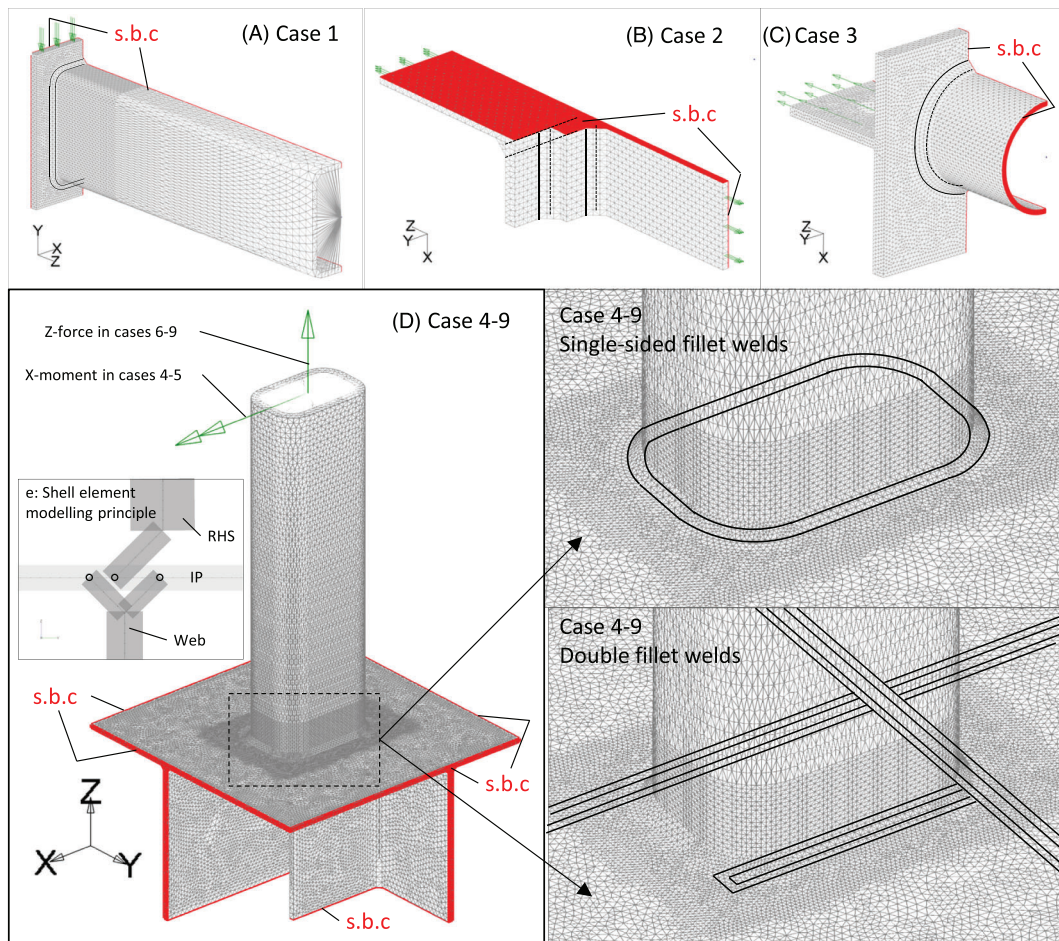


FIGURE 5 TFA models with connection lines for cases 1-9 (A-D) and principle of shell element modeling (E) [Colour figure can be viewed at wileyonlinelibrary.com]

supporting structure have symmetrical surface constraints. A load is applied to the end of the RHS profile. The RHS profile and the supporting structure are connected to the intermediate plate with fillet welds. The connection concept is the same for all of cases 4–9. The varied parameters are the thickness of the intermediate plate, the alignment of the welds, i.e., the eccentricity and loading type as shown in Table 2. The connection geometry and alignment of the welds are visualized in Figure 4D.

In cases 4 and 5, the RHS profile is loaded with an X-axis bending moment, inducing peak weld forces on those corners of the RHS profile where the adjacent shorter edge is supported by a girder. Since the local load is divided over the plate intersection area, there is no significant stress concentration at the weld. The intermediate plate thicknesses in cases 4 and 5 are 10 and 5 mm, respectively. In cases 6 to 9, the RHS profile is loaded with a tensile axial force. Because of the unsymmetrical supporting structure, a secondary bending moment is created on the RHS profile. Therefore, high local weld forces are induced on the corners of the RHS profile adjacent to the un-supported shorter edge. In cases 6 and 7, the thickness of the intermediate plate is 10 mm, thus somewhat enabling the local forces to be distributed. Compared to case 6, in case 7, the RHS profile is moved 7 mm in the XY-plane in order to create eccentricity in the connection. In cases 8 and 9, the complexity is increased even further, with a 5-mm-thick intermediate plate which does not have the capacity to distribute the local weld forces, thereby causing severe stress concentrations on the weld. The level of complexity is highest in case 9, where a thin intermediate plate is combined with an unsymmetrically positioned RHS profile according to the supporting structure. Such an arrangement causes the forces to distribute highly unsymmetrically to double fillet welds of the supporting structure.

3.2 | FE modeling

FE models are created for all nine cases with three different modeling approaches. First, TFA models are created

in which the root and toe lines are connected (Figure 3A). Then, shell element models, which are conventionally used for such structures, are created for comparison (Figure 5E). Lastly, for validation, fully connected FE models that have a continuous mesh over the weld region are created (Figure 6A).

In Figure 5, the arrows show the loading direction and the surfaces highlighted in red show the symmetry boundary conditions that were applied (s.b.c). In all the FE models, Femap 11.4.2¹⁷ was used for the pre- and post-processing and NX-Nastran 11.0.2¹⁸ as a solver.

For cases 1 to 3, structural symmetry is utilized by modeling only one quarter of the structure. The boundary conditions and loading are applied according to the test descriptions.^{14,16} In case 1, a rigid link is created at the end of the RHS profile for suppressing Y-direction translation. A Y-direction load is applied to the top face of the intermediate plate. Symmetry boundary conditions are set in the YZ and XY planes as shown in Figure 5A. In case 2, an axial load is applied to the end faces of the 6-mm plates, which are free to deform. The symmetry boundary conditions are set in the XZ and YZ planes as shown in Figure 5B. In case 3, a Z-direction load is applied to the clamping surface around the hole in the HEA200 profile web. The symmetry boundary conditions are set in the XY and XZ planes as shown in Figure 5C. In cases 4 to 9, a rigid link is modeled to the free end of the RHS profile for applying bending loads for cases 4 and 5 and an axial tensile load for cases 6 to 9. As shown in Figure 5D, symmetry boundary conditions are set in five planes of the supporting structure to enable the structure to deform as the structure would be continuous in the x, y, and z directions. The number of elements and nodes and the element type from the NX Nastran element library¹⁸ used for each model are given in Table 3. In the remaining part of this section, the element mesh is described for each case.

3.2.1 | Models for traction force approach

In order to study the effect of element size, two meshes with 2.5- and 1.25-mm elements are created with linear

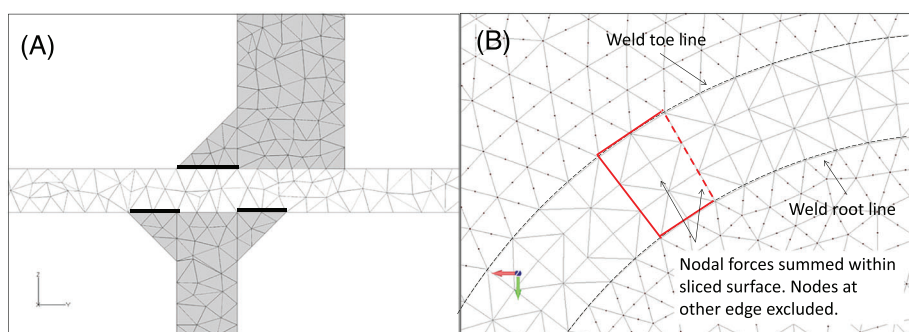


FIGURE 6 Connected nodes in full connection model and corresponding nodal force sum from sliced surface [Colour figure can be viewed at wileyonlinelibrary.com]

TABLE 3 Number of elements (nodes) in FE models with averaged values of cases 4-9 marked with *

and parabolic element types. Cases 2 and 3 are modeled with a single element size, whereas in the other cases, the areas outside the connection region are modeled with a coarser mesh using a 10-mm element size. Because of the complexity of the connections, tetrahedron elements are used to maintain good element quality. As described in Section 2, a mesh is created so that the nodes are coincident at the root and toe lines and an equal number of nodes is created on both lines. The FE mesh used for the analysis and the connected node lines are highlighted in Figure 5.

3.2.2 | Shell element model

In the shell model, elements are created in the mid-plane of the wall thickness using the principle shown in Figure 5E. For weld elements, the thickness is set to be equal to the actual weld throat thickness, and elements are modeled at half the distance of the throat thickness, as recommended by Radaj et al.¹⁹ Linear shell elements with an element size of 2.5 mm are applied. Similarly to the TFA models, cases 2 and 3 are modeled with a single element size, whereas in other cases, areas outside the connection region are modeled with a coarser mesh using a 10-mm element size. The averaged line traction force f_l and bending moment m_l are calculated as

$$f_{li,i+1} = \frac{0.5(F_i + F_{i+1})}{L_{i,i+1}}, \quad (6)$$

$$m_{li,i+1} = \frac{0.5(M_i + M_{i+1})}{L_{i,i+1}}. \quad (7)$$

3.2.3 | Full connection model

The full connection model is considered as an accurate model used for validation. The difference from TFA is that all the nodes along the weld leg are connected to the intermediate plate, as shown in Figure 6A. Otherwise, the meshes for cases 1–9 are as shown in Figure 5. In order to get a distinct value for the weld force along the weld line, the connecting surfaces are sliced into 5-mm-long sections before meshing (Figure 6B). An element size of 2.5 mm with parabolic tetrahedra is used. Again, cases 2 and 3 are modeled with a single element size, whereas in the other cases, areas outside the connection region are modeled with a coarser mesh using a 10-mm element size. In the full connection model, the nodal sum force within the sliced sections at the connection

surface is divided by the average length of the section (Figure 6B). A section-wise graph is created after all the sum forces are read. For each section, the other edge nodes are excluded from the nodal sum, thus creating the correct sum force for the given weld length. The bending moment for the section is calculated from the node forces to half the width of the weld throat section.

4 | RESULTS

4.1 | Validation of traction force approach for complex connections

The traction force approach (TFA) is validated by comparing the weld force distribution resulting from TFA to that from the full connection model. In addition to the weld force distribution plots, numerical values for the peak weld force and error percentage are shown. The analyses of the results for TFA include the linear and parabolic element models with element sizes of 1.25 and 2.5 mm. The comparisons are shown for the most relevant, i.e., heavily loaded welds, divided into single-sided and double fillet welds. All the weld force distribution plots are presented in Appendix A (Figures A1–A3), including also the degree of bending δ_b calculated as

$$\delta_b = \frac{|\sigma_{wb}|}{|\sigma_{wb}| + |\sigma_{wm}|} = \frac{\frac{6|m_l|}{L_w^2}}{\frac{1}{L_w} \left(|f_l| + \frac{6|m_l|}{L_w} \right)} = \frac{\frac{6|m_l|}{L_w}}{|f_l| + \frac{6|m_l|}{L_w}}. \quad (8)$$

4.1.1 | Single-sided fillet welds

The single-sided welds that were analyzed, together with the plotting paths, are shown in Figure 7. Case 1 is the corner of the hollow section that failed in the fatigue tests. For case 2, the fatigue-critical location is the weld between the cover plate and intermediate plate. For case 3, the failed weld in the fatigue tests was the Ø76.1 × 2.9 tube weld. Cases 4–9 have single-sided fillet welds on RHS for which the weld forces are plotted for two weld segments separately, as shown in Figure 7.

Figure 8 shows an example of a weld force distribution comparison for the Case 8 RHS weld. It can be seen that TFA can capture the force distribution and peak force value, whereas the shell element model overestimates the peak weld force value, predicting force concentrations also in unrealistic locations. The reason for this is the force concentration that occurs at each location where the shell elements intersect. Such areas are found

FIGURE 7 Direction with start and stop point for plotting results for single-sided welds [Colour figure can be viewed at wileyonlinelibrary.com]

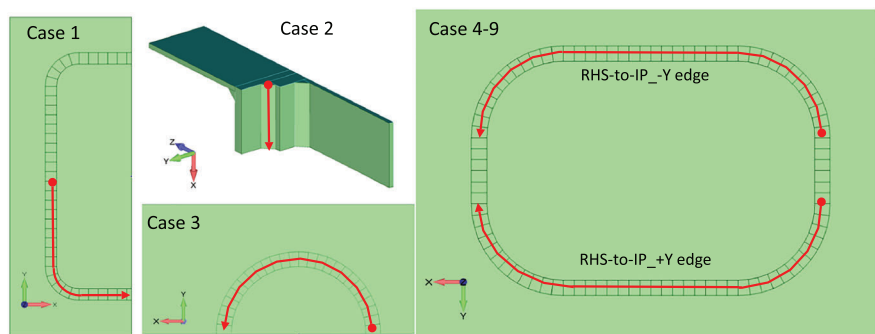
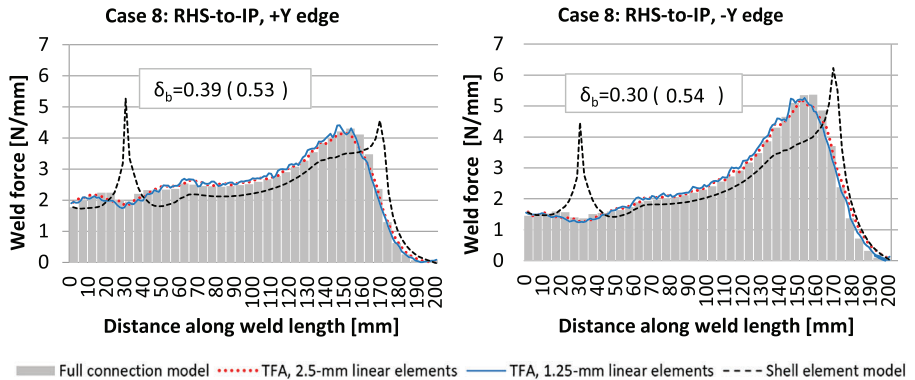


FIGURE 8 Example of weld force and degree of bending of single-sided fillet welds [Colour figure can be viewed at wileyonlinelibrary.com]



on those corners of the RHS profile where the adjacent shorter edge is supported by a girder (at the 30-mm location in Figure 8) and on those corners of the RHS profile adjacent to the unsupported shorter edge (at the 170-mm location in Figure 8). There is only a minor difference between using 2.5- or 1.25-mm elements, showing that the TFA is mesh-insensitive. Similar findings are observed for all the cases that are studied.

A summary of all the results for single-sided fillet welds is given in Table 4. Zero error is considered if the peak force along a weld line averaged for a 5-mm length is the same with the full connection model. In cases 4–9, the error is calculated for the $-Y$ -side segment that has a higher peak force. For TFA, the maximum error is 10% and the average error 4%. For the shell element model, the maximum error is 34% and the average error 13%, with only an element size of 2.5 mm being considered. In addition to proper estimation of the weld force, the traction force can be used to indicate the degree of bending δ_b . The example of the δ_b values at the peak weld force location are shown for a fully connected model result and TFA with a 2.5-mm linear element model in brackets in Figure 8. All the results are provided in Table 4, where the error for δ_b is given in percentage points. The accuracy of the bending estimation is very good in the symmetrical cases 1 to 3, with an average error of 2 pp, and reasonably good in cases 4 and 5, with an average error of 5 pp. As the complexity increases in cases 6 to

9, so does the error in the accuracy of the degree of bending, being 14 pp on average. In general, it is observed that when the actual value of degree of bending is below 0.55, the error increases to above 10 pp.

4.1.2 | Double fillet welds

Double fillet welds concern cases 4–9, namely, web, flat bar, and girder welds to an intermediate plate. The weld forces are plotted individually for the inner and outer welds of the web and flat bar, as shown in Figure 9. Since the forces at the girder welds are low, they are not shown. In the web-to-girder and flat bar-to-girder intersection area, the total force at the corner segment cannot be distinctly defined because of the intersecting welds. To overcome this issue, it is considered here that it is appropriate to define the local fatigue failure in the intersection area as a failure of the corner segment and its first adjacent segments together, as shown in Figure 9. The selected area is comparable to the one used in the case of a fillet weld around an attachment end in earlier studies.²⁰ The starting point for the weld distribution plots is set after the intersection area. In all cases, the peak forces were outside the intersection area.

Figure 10 shows an example of a comparison of the weld force distribution of an inner fillet weld of a web and flat bar in case 8; all the results are given in

TABLE 4 Error (e) (%) of fatigue critical weld force (N/mm) and error (pp) of degree of bending with varied element size and type in single-sided fillet welds

Case	1				2				3				4				5				6				7				8				9			
	Value	e	Value	e	Value	e	Value	e	Value	e	Value	e	Value	e	Value	e	Value	e	Value	e	Value	e	Value	e	Value	e	Value	e	Value	e						
Full connection model	Force	60.9	0	13.9	0	20.9	0	88.0	0	90.8	0	4.6	0	4.7	0	5.4	0	6.4	0	6.4	0	6.4	0	6.4	0	6.4	0	6.4	0	6.4	0					
	δ_b	0.70	0	0.70	0	0.73	0	0.58	0	0.52	0	0.47	0	0.53	0	0.30	0	0.55	0	0.55	0	0.55	0	0.55	0	0.55	0	0.55	0	0.55	0					
Shell model, 2.5-mm linear	Force	57.2	6	16.0	15	25.5	22	85.2	3	121.8	34	4.1	10	5.0	5	5.9	9	7.1	10	7.1	10	7.1	10	7.1	10	7.1	10	7.1	10	7.1	10					
	δ_b	0.73	3	0.73	3	0.74	1	0.64	6	0.61	9	0.62	15	0.58	5	0.54	24	0.58	3	0.58	3	0.58	3	0.58	3	0.58	3	0.58	3	0.58	3					
TFA, 2.5-mm parabolic	Force	61.9	2	14.3	3	19.2	8	85.4	3	85.5	6	4.4	4	4.4	7	5.2	3	6.1	5	6.1	5	6.1	5	6.1	5	6.1	5	6.1	5	6.1	5	6.1	5			
	Force	61.0	0	14.4	3	19.3	8	87.7	0	87.8	3	4.4	4	4.5	4	5.2	3	6.2	4	6.2	4	6.2	4	6.2	4	6.2	4	6.2	4	6.2	4	6.2	4			
TFA, 1.25-mm linear	Force	60.4	1	14.3	2	18.8	10	85.6	3	83.7	8	4.2	7	4.3	8	5.1	5	6.1	6	6.1	6	6.1	6	6.1	6	6.1	6	6.1	6	6.1	6	6.1	6			
	Force	60.4	1	14.3	2	18.8	10	85.6	3	83.7	8	4.2	7	4.3	8	5.1	5	6.1	6	6.1	6	6.1	6	6.1	6	6.1	6	6.1	6	6.1	6	6.1	6			
TFA, 1.25-mm parabolic	Force	60.4	1	14.3	2	18.8	10	85.6	3	83.7	8	4.2	7	4.3	8	5.1	5	6.1	6	6.1	6	6.1	6	6.1	6	6.1	6	6.1	6	6.1	6	6.1	6			
	Force	60.4	1	14.3	2	18.8	10	85.6	3	83.7	8	4.2	7	4.3	8	5.1	5	6.1	6	6.1	6	6.1	6	6.1	6	6.1	6	6.1	6	6.1	6	6.1	6			

Appendix A. It is observed that TFA can capture the force distribution and peak weld force in all fatigue-critical welds. For the shell element model, the peak weld force is highly overestimated for inner welds in cases 6–9, while the accuracy of the outer welds is good in all cases. The location of the peak weld force is not predicted correctly in cases 4–5 with the shell element model.

Table 5 shows the error in the peak weld force for all the double fillet welds. When the error is being defined, both welds in a double fillet weld are considered as one welded connection. Therefore, the peak force found either from the inner or outer weld defines the error of the double fillet weld. Zero error is considered if the peak force of the web and flat bar double fillet welds averaged to a 5-mm distance is the same as in the full connection model. Considering the results of a 2.5-mm linear element mesh, the maximum error for TFA is 8% and the mean error 3%. When all four different meshes for TFA are considered, the maximum error is 10% and the average error 4%. For the shell element model, the maximum error is 74% and the average error 29%. For double fillet welds, the accuracy of the degree of bending from TFA is good in all cases, with the error being on average 3 pp. All the results for δ_b are given in Table 5, where the error for δ_b is given in percentage points.

4.2 | Influence of structural complexity

As the structural complexity increases, the accuracy of the shell element model significantly decreases, while the accuracy of TFA remains same. This effect is shown in Figure 11 for single (A) and double fillet welds (B) separately. As can be seen in Figure 11A, case 1 has good accuracy in both models since it does not contain severe weld force concentrations. Case 3 already has considerable structural discontinuity since the weld of the Ø76.1 × 2.9 tube intersects with the web plate of the HEA200 profile. In case 5, in addition to intersecting welds, the connection is unsymmetrical, thus concentrating forces on those corners of the RHS profile where the adjacent shorter edge is supported by the girder. Such complexity creates a highly overestimated force concentration at the RHS corner using the shell element model.

As shown in Figure 11B for double fillet welds, the accuracy is good for both models for the outer welds since they do not contain intersecting welds that would cause severe force concentrations (see also Figure 4D). The inner welds, however, intersect with the RHS fillet weld. Also, as cases 4–9 are highly unsymmetrical, weld forces are unsymmetrically distributed along the weld length. Here, the influence on the shell element model is demonstrated for the inner web welds in cases

FIGURE 9 Direction with start and stop points for plotting results for double fillet welds [Colour figure can be viewed at wileyonlinelibrary.com]

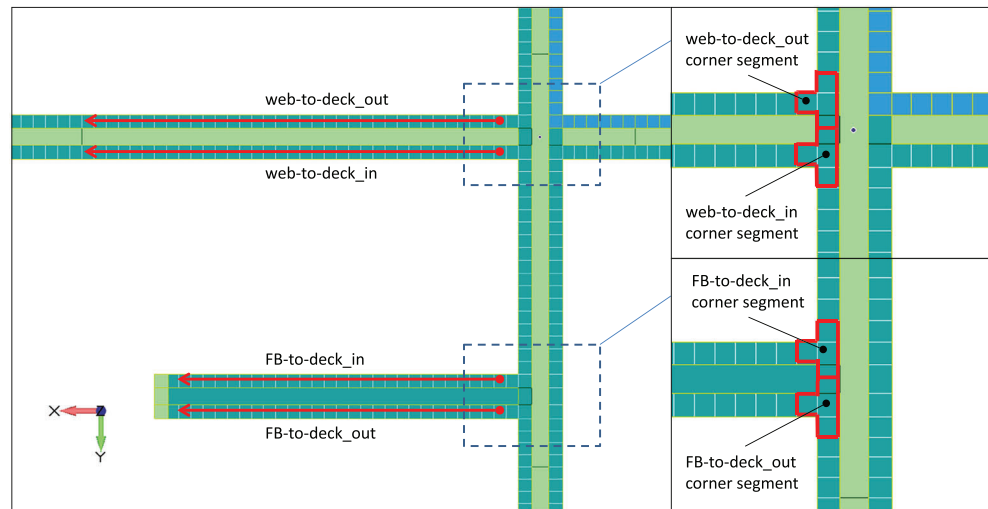
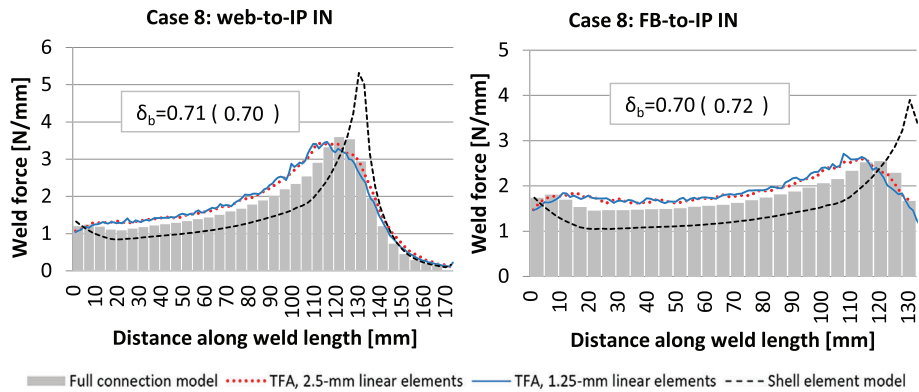


FIGURE 10 Example of weld force and degree of bending of double fillet welds [Colour figure can be viewed at wileyonlinelibrary.com]



5 and 8. The shell element model highly overestimates the peak force and predicts a wrong position for it in case 5, where intersecting welds at the $+X$ edge (see Figure 9) are estimated to have a higher local load than the web-girder intersection at the $-X$ edge. On one hand, this is because the complex load distribution on each weld is not correctly captured in the web-girder intersection area. On the other hand, the intersecting welds at the $+X$ edge create an overestimated local weld force, which is a typical effect in shell element models.

4.3 | Fatigue strength of complex load-carrying cruciform connections

Fatigue test results were reviewed for cases 1–3^{14,16} by calculating the S-N curves, standard deviation, and scatter index on the basis of the nominal weld stress and local nominal weld stress. The load ratio in the tests was $R = 0.5$ for case 1 and $R = 0$ for cases 2–3. The $R = 0$ test results are corrected to $R = 0.5$ by multiplying the stress values by a factor of 1/1.1, according to the mean

stress correction.²¹ In the nominal weld stress approach, the weld stress is calculated with beam theory, considering the actual weld throat thickness for each specimen. In the local nominal weld stress approach, the averaged weld force for a 5-mm length is calculated for each specimen using the TFA approach. In each case, 1–3, the same FE model is used for all the specimens, using the average weld throat thickness of all the specimens. The local nominal weld stress is then calculated by dividing the local weld force by the actual weld throat thickness of the corresponding specimen. To compare the effect of the complexity of the connections to the resulting S-N curves, the force concentration factor (FCF) was calculated by dividing the peak weld force by the nominal weld force.

From the results (Figure 12), it can be seen that the FAT36 design curve given in IIW, DNV-GL, and EC3 is un-conservative for the nominal weld stress approach but well suitable for the local nominal weld stress approach. In cases 1–3, the weld dimensions are as defined for the FAT36 curve in IIW, i.e., ratio of fillet weld throat thickness a_w to the thickness of a loaded plate t larger

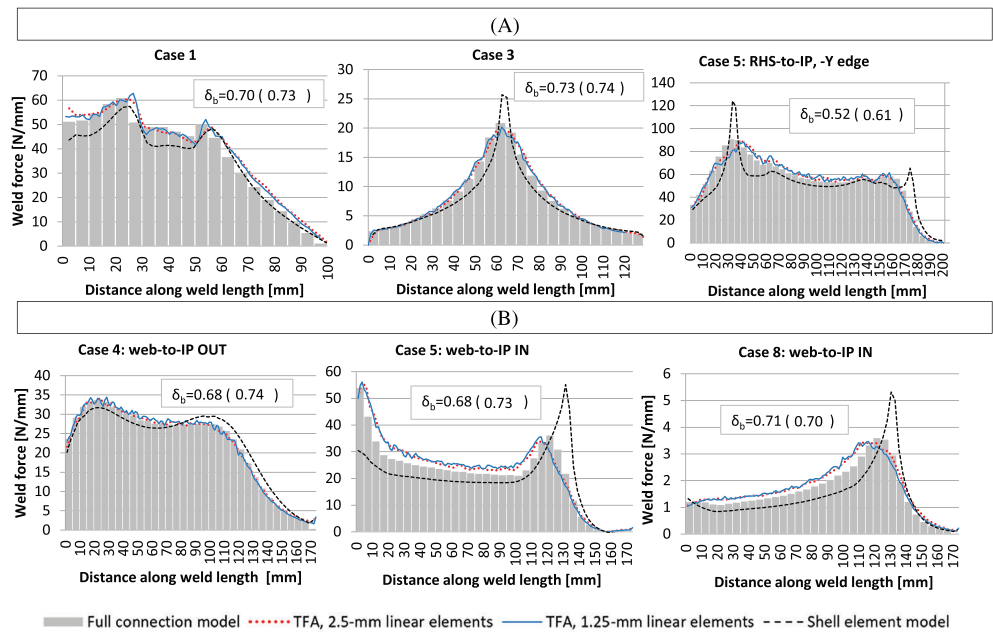
TABLE 5 Error (ϵ) (%) of fatigue critical weld force (N/mm) and error (pp) of degree of bending with varied element size and type in double fillet welds

Case	4 web				4 FB				5 web				5 FB				6 web				6 FB			
	Value	ϵ	Value	ϵ	Value	ϵ	Value	ϵ	Value	ϵ	Value	ϵ	Value	ϵ	Value	ϵ	Value	ϵ	Value	ϵ				
Full connection model	Force	33.7	0	35.2	0	53.9	0	53.6	0	0	0	0	2.0	0	2.0	0	0	0	0	0				
	δ_b	0.68	0	0.70	0	0.68	0	0.68	0	0	0	0	0.65	0	0.65	0	0	0	0	0				
Shell model, 2.5-mm linear	Force	31.7	6	33.0	6	50.8	6	46.4	13	13	20	20	2.2	11	2.2	11	11	11	11	11				
	δ_b	0.74	6	0.73	3	0.73	5	0.73	5	5	3	2	1.9	4	1.9	4	4	4	4	4				
TFA, 2.5-mm parabolic	Force	33.9	0	35.4	1	53.5	1	52.2	3	3	7	7	1.9	3	1.9	3	3	3	3	3				
TFA, 1.25-mm linear	Force	33.5	1	35.2	0	54.2	0	52.4	2	2	5	5	1.9	3	1.9	3	3	3	3	3				
TFA, 1.25-mm parabolic	Force	33.3	1	34.9	1	52.0	4	51.1	5	5	7	7	1.9	4	1.9	4	4	4	4	4				

TABLE 5 (Continued)

Case	7 web				7 FB				8 web				8 FB				9 web				9 FB			
	Value	ϵ																						
Full connection model	2.9	0	1.9	0	3.6	0	2.5	0	4.8	0	0	2.9	0	0	2.9	0	0	2.9	0	0				
	0.58	0	0.63	0	0.71	0	0.70	0	0.62	0	0	0.68	0	0	0.68	0	0	0.68	0	0				
Shell model, 2.5-mm linear	4.9	69	3.3	74	5.2	44	3.6	43	6.5	34	34	34	3.5	22	3.5	22	22	22	22	22				
	2.8	5	1.9	1	3.4	5	2.6	2	4.5	8	8	8	2.7	4	2.7	4	4	4	4	4				
TFA, 2.5-mm parabolic	0.65	7	0.67	4	0.70	1	0.72	2	0.63	1	1	0.67	1	1	0.67	1	1	0.67	1	1				
	2.7	8	1.9	1	3.4	6	2.6	3	4.5	7	7	7	2.8	2	2.8	2	2	2	2	2				
TFA, 1.25-mm linear	2.7	7	1.9	0	3.4	5	2.6	3	4.5	7	7	7	2.8	3	2.8	3	3	3	3	3				
TFA, 1.25-mm parabolic	2.6	10	1.8	2	3.4	5	2.7	6	4.4	9	9	9	2.8	2	2.8	2	2	2	2	2				

FIGURE 11 Shell element model and TFA error for increasing complexity of connection, single-sided fillet welds (A) and double fillet welds (B) [Colour figure can be viewed at wileyonlinelibrary.com]



than 1/3. In case 3, in addition to the fillet weld, weld penetration was also present.

The scatter range index T_σ was calculated according to Radaj et al.¹⁹ using a 10% and 90% probability of survival with an S-N curve slope $m = 3$. The resulting scatter range index is $T_\sigma = 3.71$ for the nominal weld stress and $T_\sigma = 1.98$ for the local nominal weld stress. It is worth noting that these results for the local nominal weld stress match well with the results calculated with full connection models, which result in a scatter range index $T_\sigma = 1.89$. From the nominal weld stress results, it can be seen that there is a high scatter between each case with a different level of FCF, whereas in the case of the local nominal weld stress, this scatter is clearly smaller.

5 | DISCUSSION

The cases to validate the traction force approach (TFA) were selected to be such that the complexity of the case connection gradually increased. The simplest connection, i.e., case 1, did not contain any structural discontinuities that would influence the nominal weld stress. At the next level of complexity, i.e., cases 2–3, symmetrical connections included a sharp stress concentration resulting from intersecting welds over the intermediate plate. The highest level of complexity, i.e., cases 4–9, contained an unsymmetrical arrangement of scantlings, eccentricity, and intersecting welds over the intermediate plate. Cases 4–9 have great significance since research is typically focused on simplified and symmetrical connections, and yet cases 4–9 represent a realistic structural design in a

steel structure industry such as shipbuilding. In actual steel structures, there is always also a certain amount of eccentricity between connected plates. In previous research, this behavior has been studied with 2D cases for which analytical formulae can also be found for fatigue analysis.²² In the present paper, a rather severe 7-mm eccentricity was included in cases 7 and 9.

When the effect of the thickness of the intermediate plate is studied, it can be seen that the peak weld force of fatigue-critical welds increases up to 37% in single-sided fillet welds and up to 67% in double fillet welds when thickness is decreased from 10 to 5 mm. On the other hand, when the effect of eccentricity is studied, it can be seen that the peak weld force of fatigue-critical welds increases by up to 35% when the eccentricity is increased from 0 to 7 mm.

The traction force approach introduced in this paper requires small pre-processing effort in FE analysis as, typically, 3D geometry with fillet welds is available for FE modeling. The required modeling routine is first to merge the weld geometry with the abutting structural member and to imprint the weld toe and root lines to the surfaces of the weld leg and intermediate plate. After this, an equal number of nodes is set to the toe and root lines and coincident nodes merged on these lines. As all the nodes to be merged are associated with the root and toe line geometries, the merging of the correct nodes by using the line geometries is easy. In the post-processing phase, the location of the peak weld force is easy to detect from the nodal forces of the two lines and the peak force value is easy to define from the node distances (see the equations in Table 1). If the nodal forces

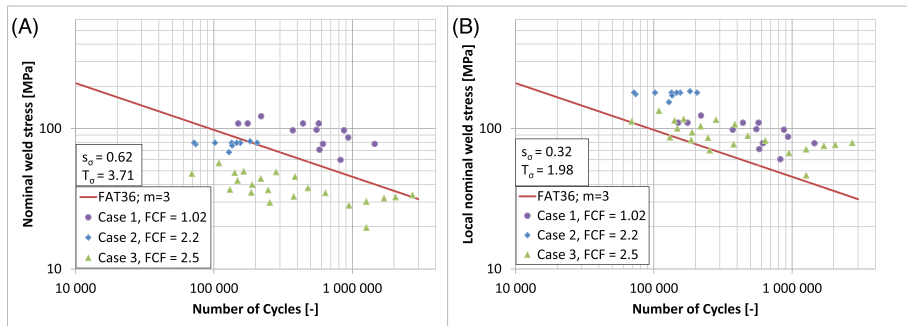


FIGURE 12 Literature fatigue test data, nominal weld stress (A) and local nominal weld stress (B) [Colour figure can be viewed at wileyonlinelibrary.com]

and node coordinates along the weld length are provided in tabular format, it is rather easy to create a weld force distribution plot using these equations. A weld force distribution plot reveals the weld force gradients, which are an important measure for the designer in optimizing the connection.

Fully connected modeling with 3D solid elements or a 2D element is a well-known approach, as used for weld root analysis, e.g., by Fricke.¹⁴ For weld toe structural stress analysis, it has been widely used, e.g., by Dong.²³ Another approach utilizing nodal forces and fully connected modeling is the traction structural stress approach.¹⁵ With that approach, meshing needs to be controlled by mapped meshing to create element lines across the weld throat thickness and across the plate thickness at the weld toe. The mesh also needs to be controlled in the longitudinal direction of the weld to have planar element lines in each cross-section along the weld. Therefore, the disadvantage is that in a complex 3D connection such as that presented in Figure 4D such mesh mapping is extremely time-consuming. In the proposed TFA approach, the mesh controlling is not so strict as the only requirement is to have an equal number of nodes on the weld toe and root lines.

In complex 3D connections, including many welds pre- and post-processing becomes challenging for all approaches that require fully connected modeling technique. In the pre-processing phase, special attention is required in merging the nodes because of the unfused root surfaces. The other challenge is that for detecting the peak load location and defining a distinct force/mm value the weld leg surface needs to be sliced into sections with a specific length, e.g., 5 mm, as was done in this paper (Figure 6B). Creating weld force plots also requires a more complex code than for TFA as in addition to the weld line axis, the axis in the thickness direction also needs to be included. Moreover, compared to straight welds, the pre- and post-processing work becomes even more challenging when the weld line is curved. Since in the connection optimization process multiple concepts are typically tested, significant savings in the total

analysis time can be achieved by using the traction force approach.

Similarly to other traction force-based approaches,^{15,23} the TFA presented in this paper was found to be mesh-insensitive since with the four different meshes; i.e., varying element size and types, on average, the maximum difference between the peak weld force of the fatigue-critical welds was 3%. Considering the fatigue-critical welds in cases 1–9, the maximum error in the TFA approach was 10%. For single-sided fillet welds, the highest error was found in cases 3 and 9. In these cases, there was also a severe force concentration. Looking at cases 1–3, the highest force concentration factor (FCF) was in case 3, with an FCF of 2.5. For cases 4–9, the highest FCF of 2.8 is found for case 9. In the double fillet welds, the highest error was at the web-to-IP weld in cases 7 and 9, with eccentricity of 7 mm. The highest peak force was found for case 9, and yet the connection between the magnitude of error and the magnitude of the peak force is not as clear as with single-sided fillet welds. In addition to the correct peak force of the fatigue-critical weld, i.e., a weld with a higher loading, TFA is able to capture the load ratio of the inner and outer welds.

A comparison between the nominal and local nominal weld stress for the fatigue test results in cases 1–3 showed that the local nominal weld stress approach results in more reliable fatigue life estimations with a smaller scatter range index ($T_\sigma = 1.98$). This is a well-expected result since fatigue failures originate from the stress concentrations where the stress is highest. Stress concentrations are not included in the nominal weld stress approach, which is reflected as a higher scatter in fatigue test results. These test points are also logically distributed over the S-N plot since the points in case 3 with the highest FCF, i.e., 2.5, have the lowest fatigue strength when analyzed with the nominal weld stress approach. Case 2, with FCF = 2.2, has higher fatigue strength, and case 3, with FCF = 1.02, has clearly the highest fatigue strength. Despite the clear improvement in scatter from the nominal to the local nominal weld stress approach,

the scatter is still somewhat higher than for simple welded connections where $T_\sigma = 1.5$ has been observed for weld toe failures by, e.g., Meneghetti.²⁴ This is a similar observation to that of Meneghetti et al.⁸ using a peak stress approach. Higher scatter is observed for three-dimensional welded connections than for simple small-scale specimens of welded joints. The results also show that FAT36 found from standards and recommendations for analysis based on the nominal weld stress match the local nominal weld stress results well. On the other hand, over half of the test data falls below FAT36 with the nominal weld stress approach. It is worth noting that all the test series had almost equal degrees of bending, varying between 0.70 and 0.73.

The accuracy of the shell element models was very poor, as error up to 74% was detected. Only the outer double fillet welds that do not intersect with RHS welds were found with good accuracy. One example of the instability of shell element models is the RHS-to-IP welds in cases 4 and 5. Case 4 has good peak weld force accuracy even though the force distribution is not correct. However, just as a result of changing the thickness of the intermediate plate from 10 to 5 mm in case 5, the peak weld force error increases drastically. This is because modeling with mid-plate elements creates the weld lines at a different position in the two cases. Thus, in case 5, the RHS welds more clearly intersect with a double fillet weld, thus creating an unrealistically high force concentration. Generally, in welds that intersected with RHS welds, the error was high. In such cases, there were also weld force peaks in unrealistic locations. The validity of the shell element's plane stress assumption was verified in the cases that were studied since the stress in the thickness direction is negligible compared to the stresses in the loading direction. The aforementioned challenges in the stress calculations make the utilization of the shell model impossible in the automated analysis routines required for structural optimization. Using TFA, these challenges are removed, and there is still analytical efficiency and the possibility of automated meshing and analysis. It is also worthy of note that TFA can predict the degree of bending in the weld leg section. This information can be used as an indicator in optimizing the connection since a lower degree of bending results in higher fatigue strength through structural stress analysis if the local weld force is kept the same.

In the simplest case that was studied, case 1, the connection type was a single-sided load carrying a cruciform connection with only a very light weld force concentration along the weld. This suggests that the approach is also suitable for analyzing 2D cross-sections of simple load-carrying cruciform connections which also do not consider any force concentrations along the weld.

However, compared to a full connection model, the time saving with TFA in such connections is not as significant as with complex 3D connections. In such connections, in addition to weld root fatigue, another possible failure mode is weld toe fatigue, which can be analyzed with the well-accepted structural hot spot approach.^{1,3} Alternatively, the TFA introduced here can also be validated for the analysis of weld toe failure. This is beyond the scope of current study, and thus, this is left for future work.

The connections studied in this paper were axially loaded, and thus, the effect of longitudinal shear stresses is small compared to stress components in the loading direction. However, the traction force approach can also be used to calculate the longitudinal shear stress for cases where shearing effects need to be considered. This topic is left for future work.

6 | CONCLUSION

This paper introduced a new traction force approach (TFA) for efficient fatigue analysis of load-carrying cruciform connections in large complex structures. The validation of TFA was performed by comparing the results with a full connection solid element model that had a realistic connection over the welds. Furthermore, the fatigue scatter was compared using a nominal weld stress approach and a local nominal weld stress approach obtained by TFA. Based on the present study, the following conclusion can be drawn:

- The TFA, connecting the welded parts only from the toe and root lines, can correctly and efficiently define local peak weld forces for the complex welded connections. The maximum peak force error of fatigue-critical welds was 10%, with the average error being 4%. Furthermore, the approach was found to be independent of element size and formulation.
- For complex welded connections, traditionally used shell element models show severe challenges in capturing the correct weld forces, as the maximum peak force error of fatigue-critical welds was 74%, with the average error being 22%. This was due to shell element's improper modeling of local stiffness in the area of intersecting welds.
- The fatigue analysis based on local weld forces using TFA reduced the scatter range index from 3.71 to 1.98 when compared to a nominal weld stress approach, showing that TFA can result in reliable fatigue strength predictions.
- When TFA is compared to the alternative full connection model, significant analysis time savings can be

achieved in the pre- and post-processing phases for complex connections.

In this paper, the TFA was validated for complex fillet welded joints under axial loading. In order to validate the approach for other joint types and weld profiles, e.g., fillet welds with significant weld penetration, further study is needed. Furthermore, the shear-loaded connections need to be considered as future work.

ACKNOWLEDGMENTS

This research was funded by Meyer Turku Oy. The financial support is gratefully acknowledged. Sincere thanks to Prof. Jani Romanoff for his valuable comments on the paper.

DATA AVAILABILITY STATEMENT

The authors elect to not share data.

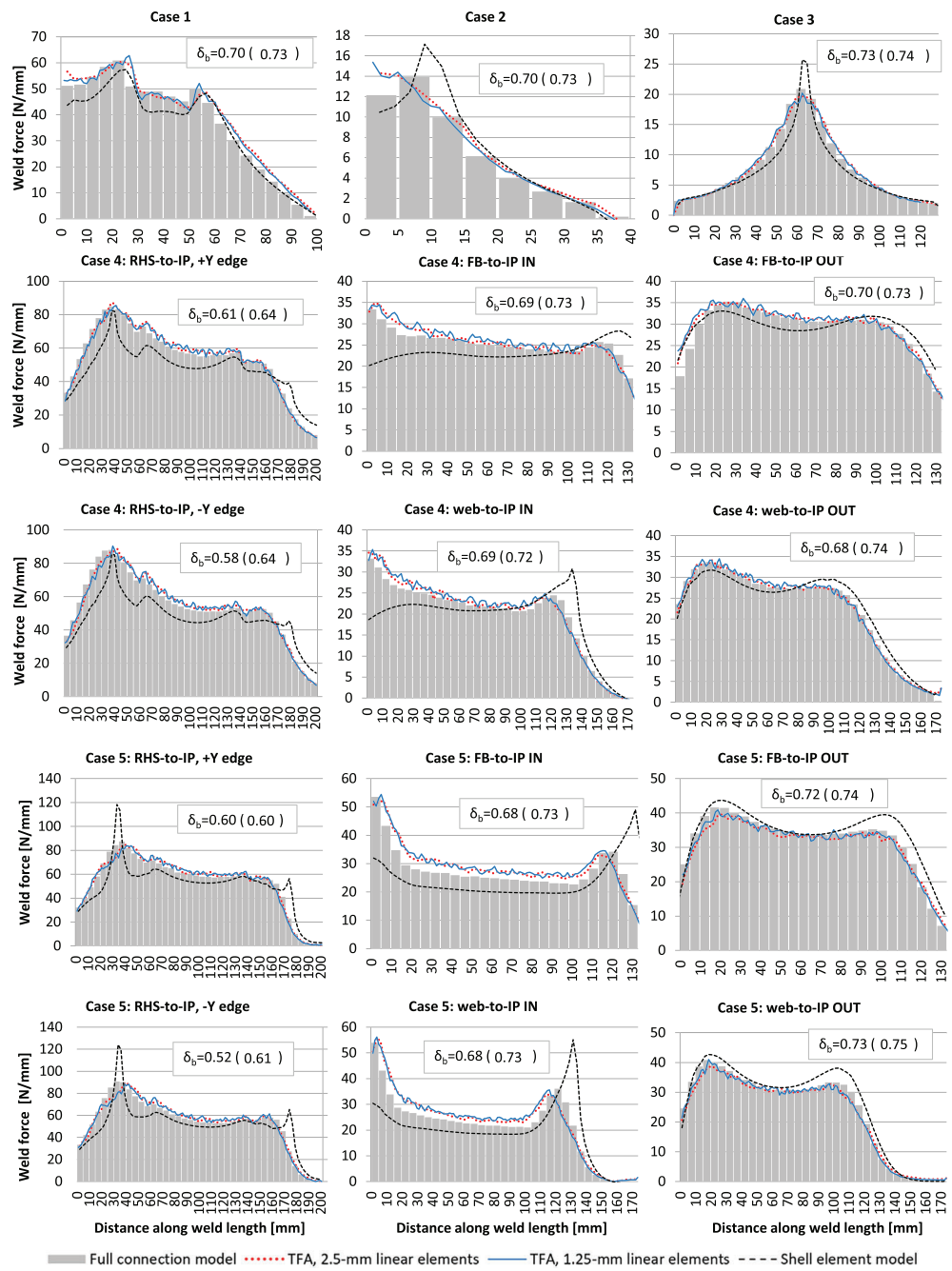
ORCID

Matti Rautiainen  <https://orcid.org/0000-0001-6504-9188>

REFERENCES

1. Eurocode 3, Design of steel structures, Part 1-9, Fatigue, EN 1993-1-9, Brussels, CEN, 2006.
2. DNV-GL. DNVGL-RP-C203. Fatigue design of offshore steel structures. 2014 06:/201.
3. DNV-GL. DNVGL-CG-0129. Fatigue assessment of ship structures. 2018 01:/236.
4. Hobbacher AF. *Recommendations for Fatigue Design of Welded Joints and Components*. Cham: Springer; 2016.
5. Fricke W. IIW guideline for the assessment of weld root fatigue. *Weld World*. 2013;57(6):753-791.
6. Fricke W, Bollero A, Chirica I, et al. Round robin study on structural hot-spot and effective notch stress analysis. *Ships Offshore Struct*. 2008;3(4):335-345.
7. Fricke W, Codda M, Feltz O, et al. Round robin study on local stress and fatigue assessment of lap joints and doubler plates. *Ships Offshore Struct*. 2013;8(6):621-627.
8. Meneghetti G, Guzzella C, Atzori B. The peak stress method combined with 3D finite element models for fatigue assessment of toe and root cracking in steel welded joints subjected to axial or bending loading. *Fatigue Fract Eng Mater Struct*. 2014;37(7):722-739.
9. Foti P, Berto F. Fatigue assessment of high strength welded joints through the strain energy density method. *Fatigue Fract Eng Mater Struct*. 2020;43(11):2694-2702.
10. Foti P, Santonocito D, Risitano G, Berto F. Fatigue assessment of cruciform joints: Comparison between strain energy density predictions and current standards and recommendations. *Eng Struct*. 2021;230:111708.
11. Carpinteri A, Ronchei C, Scorza D, Vantadori S. Fracture mechanics based approach to fatigue analysis of welded joints. *Eng Fail Anal*. 2015;49:67-78.
12. Remes H, Gallo P, Jelovica J, Romanoff J, Lehto P. Fatigue strength modelling of high-performing welded joints. *Int J Fatigue*. 2020;135:105555.
13. Sorensen J, Tychsen J, Andersen J, Brandstrup R. Fatigue analysis of load-carrying fillet welds. *J Offshore Mech Arct Eng*. 2006;128(1):65-74.
14. Fricke W. Fatigue assessment of root cracking of fillet welds subject to throat bending using the structural stress approach. *Weld World*. 2006;50(7):64-74.
15. Wang P, Pei X, Dong P, Song S. Traction structural stress analysis of fatigue behaviors of rib-to-deck joints in orthotropic bridge deck. *Int J Fatigue*. 2019;17:11-22.
16. Krenzel M. Fatigue strength of a welded tube-to-plate joint at an offshore structure [dissertation]. University of Southern Denmark; 2019.
17. Femap. User Guide Version 11.4.2
18. NX Nastran. 11.0.2 Release Guide
19. Radaj D, Sonsino C, Fricke W. *Fatigue Assessment of Welded Joints by Local Approaches*. 2nd ed. Cambridge: Woodhead Publishing; 2006.
20. Fricke W, Doerk O. Simplified approach to fatigue strength assessment of fillet-welded attachment ends. *Int J Fatigue*. 2006;28(2):141-150.
21. Sonsino CM. A consideration of allowable equivalent stresses for fatigue design of welded joints according to the notch stress concept with the reference radii $r_{ref} = 1.00$ and 0.05 mm. *Weld World*. 2009;53(3-4):64-75.
22. Xing S, Dong P. An analytical SCF solution method for joint misalignments and application in fatigue test data interpretation. *Mar Struct*. 2016;50:143-161.
23. Dong P. A structural stress definition and numerical implementation for fatigue analysis of welded joints. *Int J Fatigue*. 2001;23(10):865-876.
24. Meneghetti G. The peak stress method applied to fatigue strength assessments of load carrying transverse fillet welds with toe or root failures. *Struct Durability & Health Monit*. 2012;8(2):111-130.

How to cite this article: Rautiainen M, Remes H, Niemelä A. A traction force approach for fatigue assessment of complex welded structures. *Fatigue Fract Eng Mater Struct*. 2021;1-21. <https://doi.org/10.1111/ffe.13548>

APPENDIX A: WELD FORCE PLOTS


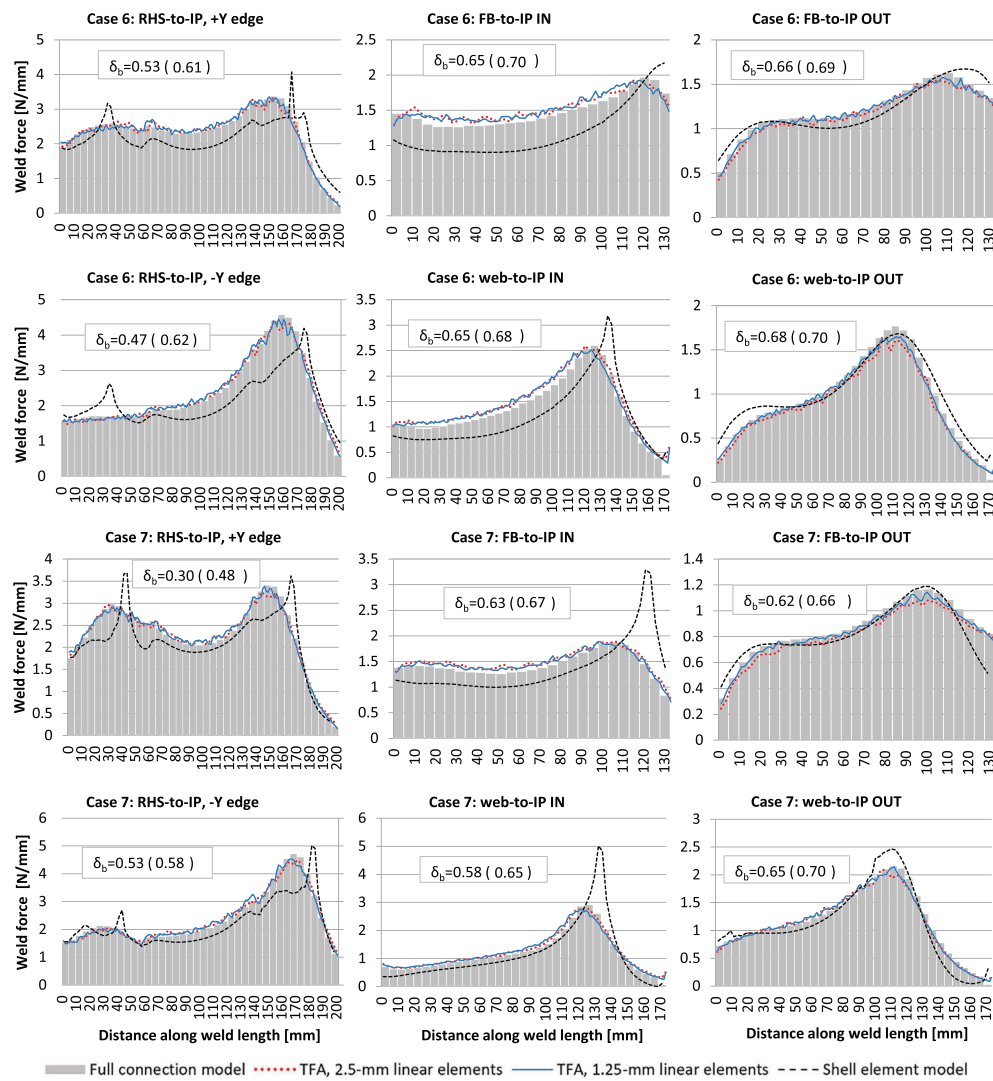


FIGURE A2 Weld force distribution plots for cases 6–7
[Colour figure can be viewed at wileyonlinelibrary.com]

FIGURE A3 Weld force distribution plots for cases 8–9
[Colour figure can be viewed at
wileyonlinelibrary.com]

